THE ASTROPHYSICAL JOURNAL, 459:342–346, 1996 March 1

TEMPERATURE STRUCTURE OF SOLAR ACTIVE REGIONS

TSUYOSHI YOSHIDA AND SAKU TSUNETA
Institute of Astronomy, The University of Tokyo, Mitaka, Tokyo 181, Japan
Received 1995 May 15; accepted 1995 August 24

ABSTRACT

We obtain high-quality temperature maps of solar active regions observed by the *Yohkoh* Soft X-ray Telescope. The temperatures of active region structures range from 3 MK to 10 MK. The bright X-ray loops do not necessarily have high temperatures, and faint structures sometimes have temperatures as high as 6 MK. The loop structures with shorter lifetimes (less than a few hours) generally have higher temperatures (5–8 MK) than the loops with longer lifetimes (3–4 MK). The plasma with temperature reaching 6–7 MK has cusp structures like solar flares (mini-cusp) or has multiple loop structures in the temperature maps in most cases. The 6–7 MK plasma is transiently heated either by magnetic reconnection at the neutral sheet above the cusp structures, or by magnetic reconnection of multiple loops. The 3–5 MK plasma is more steadily and uniformly heated. Two different mechanisms are apparently involved in the coronal heating.

Subject headings: MHD — Sun: activity — Sun: corona — Sun: fundamental parameters — Sun: X-rays, gamma rays

1. INTRODUCTION

Skylab and *Yohkoh* X-ray images of the Sun show ubiquitous bright loops (e.g., Orrall 1981; Arndt, Habbal, & Karovska 1994; Acton et al. 1992). These loop structures represent coronal magnetic structures, and the solar corona consists of these isolated magnetic loops (as well as unipolar fields). The X-ray loops apparently have a wide range of timescales. For instance, the transient brightenings (microflares) have durations from 1 to 10 minutes (Shimizu et al. 1992, 1994; Shimizu 1995). There are also steady loops with lifetimes longer than a few hours. Kano & Tsuneta (1995a, b) obtained the temperature profiles along these steady loops with lifetimes longer than a few hours and found a simple relation (a scaling law) among properties of the loops: peak temperature, density, and loop length (e.g., Rosner, Tucker & Vaiana 1978).

All the analyses made so far on the temperature structure of the coronal loops concentrated on the individual extreme-ultraviolet (EUV) and X-ray loops (Arndt et al. 1994, and references therein; Kano & Tsuneta 1995a, b; Yoshida et al. 1995; Tsuneta et al. 1992; Tsuneta 1996). However, we need to remember that the high-temperature corona apparently exists outside the distinct loops and in the diffuse region. The fundamental questions in the context of coronal heating are why specific magnetic structures are bright in X-rays, and what the difference is between bright X-ray loops and faint diffuse regions, where we do not see any distinct coronal structures (Tsuneta 1994). As a first step to answer observationally these questions, we obtain high-quality temperature maps of the *entire* active regions from X-ray maps summed over ~60 minutes by sacrificing the time resolution.

2. OBSERVATIONS AND ANALYSIS

2.1. *Observations*

The temperatures of active regions are obtained using a pair of broadband filters. We use the *Yohkoh* soft X-ray images taken from 1992 April 30 through July 5. During this period, the Soft X-ray Telescope (SXT) aboard *Yohkoh* took images of 5′ × 5′ regions around the brightest point of several active regions every ~1 minute with two different filters alternately (thin and thick aluminum filters in these particular observing periods), while taking whole Sun images with a slower cadence. The exposure time is optimized with the on-board computer to give proper signal level for each filter. Thus, the average number of incident photons is similar for the two filters, though the throughputs of the two filters are different.

We sum the images for each filter in unit of spacecraft orbit period (~97 minutes). The number of frames taken in about 60 minutes of the spacecraft daytime ranges from ~30–200 frames for each filter, depending on the operation mode of the satellite and the availability of NASA Deep Space Network downlinks. The summation allows us to obtain high-quality temperature maps even outside the bright loops (diffuse active region corona) at the expense of the time resolution.

We assume that the plasma is isothermal in a pixel (2″.46) for this analysis. The temperature maps are obtained from the ratio of the two images taken with different filters. Figure 1 (*dotted lines*) shows the relation between the ratio and the temperature. The derived temperatures do not depend on the emission measure (density) because of the assumption of the isothermality. The temperatures presented in this paper are the mean temperatures within 1 pixel, if there are multitemperature components in a single pixel. The temperatures obtained here are also time-averaged temperatures, if there is time variation in temperature during the integration period. Note that there is no systematic artifact in the temperature maps, even if there is time variation during the summation. This is simply because the images with thin and thick aluminum filters were interleavingly taken with about a 1 minute interval.

2.2. *Statistics Error in the Derived Temperatures*

Although the signal-to-noise ratio is improved by the summation of multiple frames, photon statistics is sometimes not enough for faint corona outside bright loops in active regions. The estimation of the photon statistics error in the derived temperatures is done on the basis of the analytical framework given by Kano & Tsuneta (1995a).

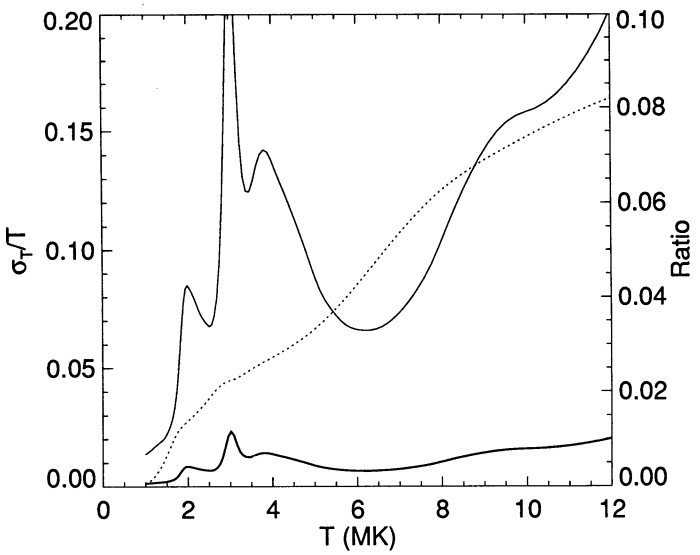

FIG. 1.—The 1 σ error in the derived temperature with a pair of broad-band filters as a function of the temperature. The thin line indicates the error in the derived temperature if the ratio of a pair of images with two filters (thin and thick aluminum filters) has 10% error. The thick line indicates the error in the derived temperature if the ratio has 1% error. The dotted line shows the relation between the temperature and the ratio of the two images.

A single incident photon of 1 keV produces about 330 photoelectrons, which is converted to the data number of about 3 DN (1 DN $\sim$ 100 photoelectrons). The DN numbers of the two images taken with different filters are almost the same owing to the optimization of the exposure time for each filter. Ten percent photon statistics error in the filter ratio, thus, corresponds to a single pixel intensity of 600 DN. Figure 1 shows the error in temperature as a function of the derived temperature, when the ratio is assumed to have 1% and 10% error. The error in temperature is temperature dependent. One percent and 10% errors of the filter ratio give maximum 1.5% and 15% errors in the derived temperatures for the range from 4 MK to 9 MK.

When the single-pixel signal is less than a threshold of 600 DN, the spatial resolution of the temperature maps is reduced intentionally to make the coarse-pixel signal higher. The error in the temperature corresponding to the threshold count of 600 DN is given by the line of 10% error in Figure 1. The bright X-ray loops which have greater than 10^4 DN in the summed images have the error of about 1%–3% in the derived temperature. The dark diffuse regions which have 10^3 DN in the summed images have about 10% error. We can also judge the quality of the temperature maps from the continuity of temperatures in adjacent pixels. The temperature map appears to be slightly noisy for areas with low signal-to-noise ratio.

We estimate the effect of the scattered photons on the temperature in an analysis of dark regions. The scattering is caused by the microroughness of the grazing incidence X-ray mirror and is represented by the power-law wing of the point-spread function. Hara et al. (1994) obtained an analytic form of the wing component using the in-flight flare data. We estimate the number of the scattered photons from bright regions with the wing component of the point-spread function given by Hara et al. (1994). The dynamic range between the bright loops and the dim corona in active regions is more than 3 orders of magnitude, and we find that the scattered photons to dark regions from bright loops are not negligible in the temperature analysis, even without flares. Therefore, we do not perform the temperature analysis for areas in which the estimated contamination signal is more than 10% of the observed signal. These areas are left blank in the temperature maps presented in this paper.

Figure 2 (Plate 11) shows the soft X-ray, temperature, electron density, and gas pressure maps, and Figures 3–6 (Plates 12–13) show the soft X-ray and the temperature maps. Electron density n_e and gas pressure p are derived from temperature T and emission measure EM; $n_e = (EM/V)^{1/2}$, and $p = 2nk_B T$, where V is the volume corresponding to a single SXT pixel (2.″46 × 2.″46) and k_B is the Boltzmann's constant. We assume that the line-of-sight thickness 2×10^9 cm throughout the analysis; $V = 6 \times 10^{25}$ cm^3.

3. TEMPERATURE STRUCTURE OF ACTIVE REGIONS

3.1. *Soft X-Ray Images and Temperature Maps*

Figure 2 shows temperature maps from 13 UT on 1992 April 30 through 1 UT on 1992 May 2. Although the observations were continuous, we show the maps with a time interval of half a day. We notice immediately from the figure that the soft X-ray maps and temperature maps appear quite different. For instance, Figure 2*d* shows a few loops with similar lengths (marked by S) around the center of the active region. The temperature maps of this region appear different. The temperature is rather uniform, and it is hard to identify these loop structures in the temperature maps: the loops appear to lose their identity in the temperature map. This indicates that the bundle of loops is heated quasi-uniformly rather than selectively. The temperature of this region appears almost constant over a day (Figs. 2*b*–2*d*). On the other hand, loops labeled D located south of the active region are transiently heated to around 5.5 MK, while loops labeled S in the center of the active region stay at 4.5 MK. One sigma error in temperature owing to the incident photon statistics is about 0.1 MK in this particular case, and the difference in temperature is significant.

The region labeled A in Figure 2*a* is low X-ray intensity diffuse corona but has temperatures of about 6 MK. This source also appears to be transient (with time resolution of 97 minutes), because this high-temperature source decays in the next two or three frames (see Fig. 7 [Plates 14–15]). We also notice a remarkable cusp labeled B with temperature of 6.5 MK in the west of Figure 2*a*. The cusp can be seen more clearly in the temperature map. Figure 2*b* also shows cusp C with temperature of 6.5 MK. (The cusp C appears again after the disappearance of the cusp B.) The temperatures of the cusp structures are generally higher than 6 MK, and the outer edge of the cusp has higher temperature.

In Figure 2*c*, the temperatures of all the loop structures are as low as 3–4 MK. We cannot identify any loop structure corresponding to the soft X-ray loops in the temperature map: there is little difference in temperature among the loops seen in the X-ray image. Again, all the loop structures in the active region lose their identity in the temperature map.

We notice that the temperatures of the loop-top regions (4.5 MK) are higher than those of the footpoints (3 MK) from Figure 2*c*. This is consistent with Yoshida et al. (1995)

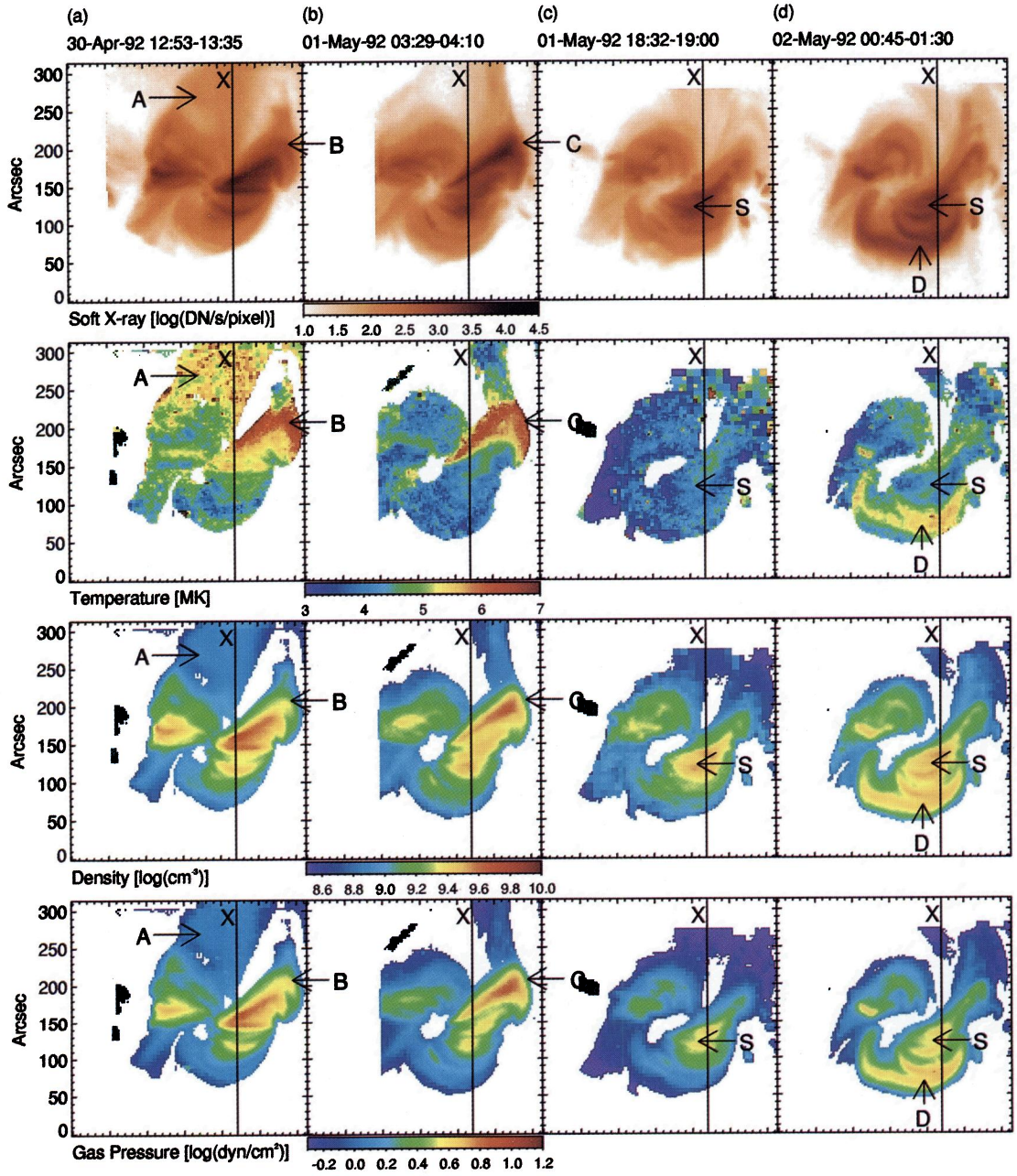

FIG. 2.—Soft X-ray (thin aluminum filter), temperature, electron density, and gas pressure maps of an active region on the center of the solar disk from 1992 April 30 through May 2. The soft X-ray maps are produced by summing frames over 60 minutes. The times shown at the top of each panel are the start and end times of the summation. The temperatures were derived from the two summed images with different analysis filters.

YOSHIDA & TSUNETA (see 459, 343)

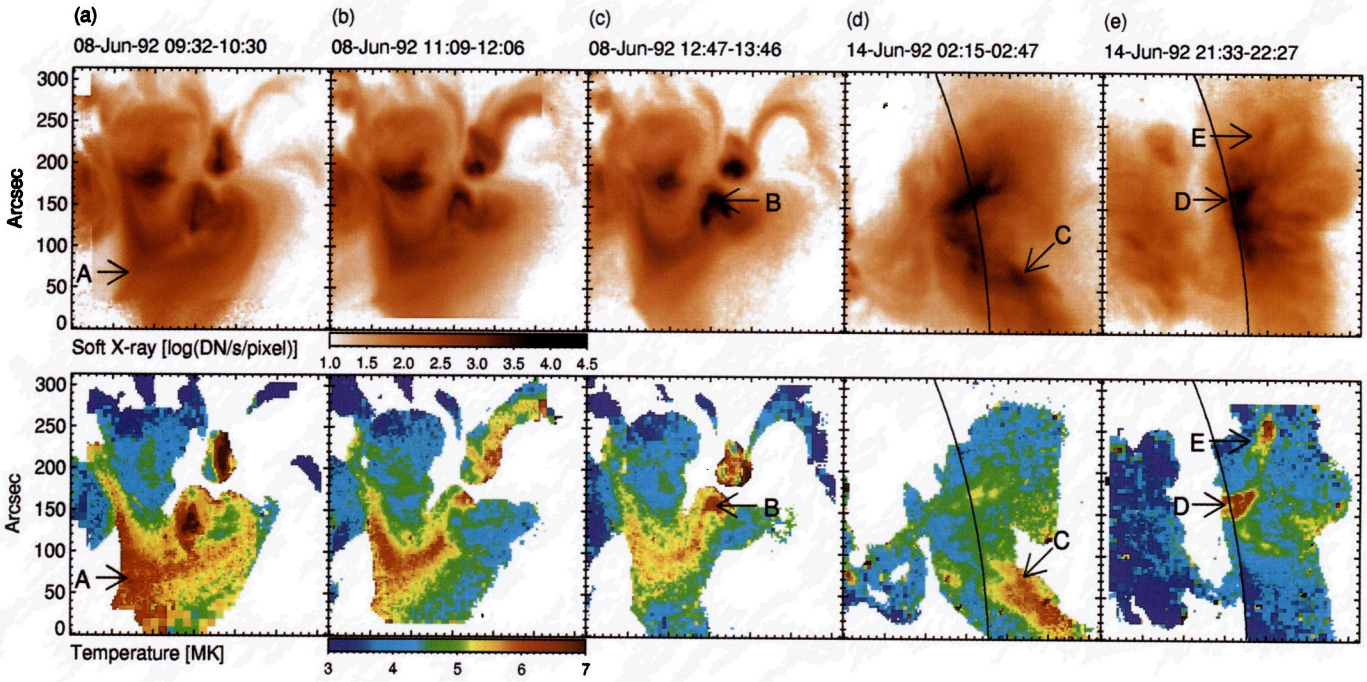

FIG. 3

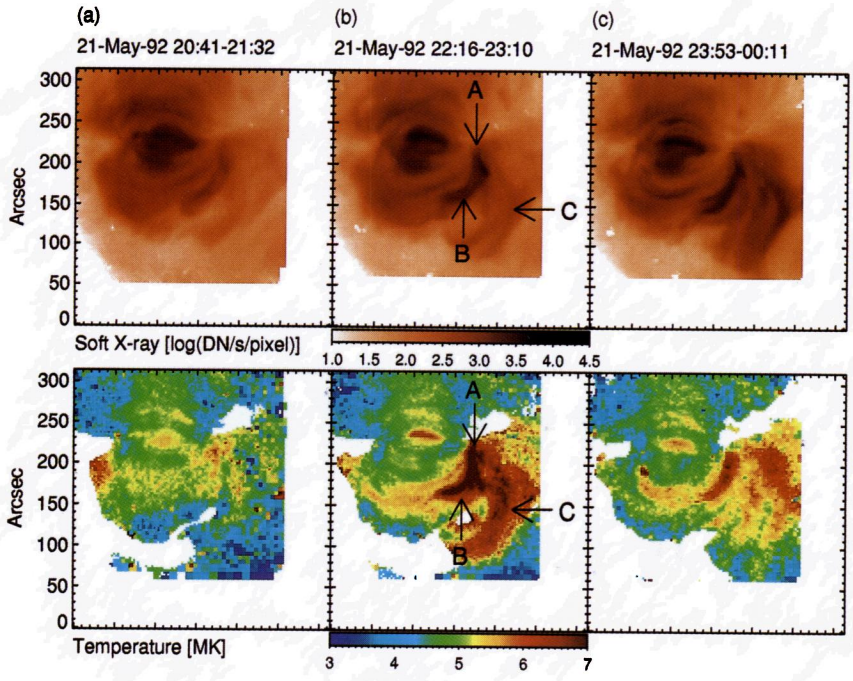

FIG. 4

FIG. 3.—Soft X-ray (thin aluminum filter) and temperature maps of an active region on 1992 June 8 and 14. The cusp structure is seen in (*a*–*c*). Small cusps are seen in (*d*), and two small cusps on the limb are seen in (*e*). These cusps are heated up to 6–7 MK. The solar limb position is shown by the black line.

FIG. 4.—Soft X-ray (thin aluminum filter) and temperature maps of an active region on 1992 May 21. The pointlike transient brightening occurred at position A, and multiple loops (B and C) with their footpoints located close to the position A are heated to 10 MK (loop B) and 7 MK (loop C).

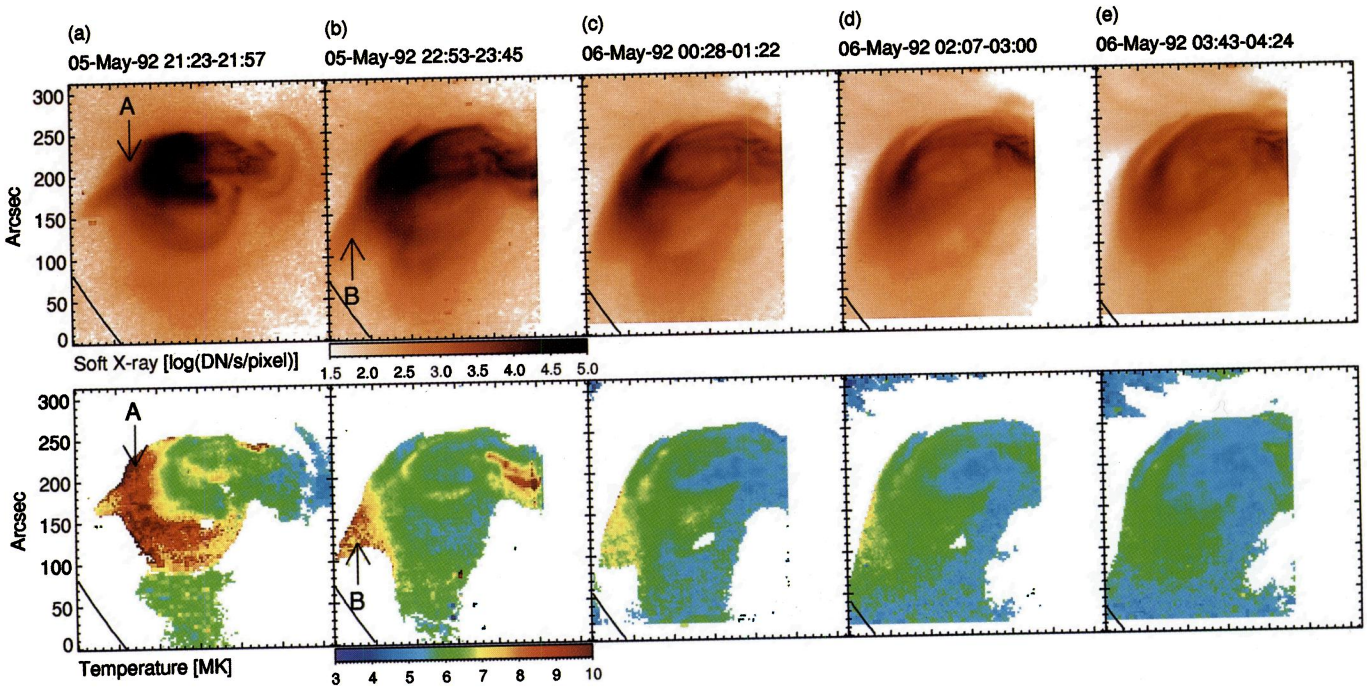

FIG. 5

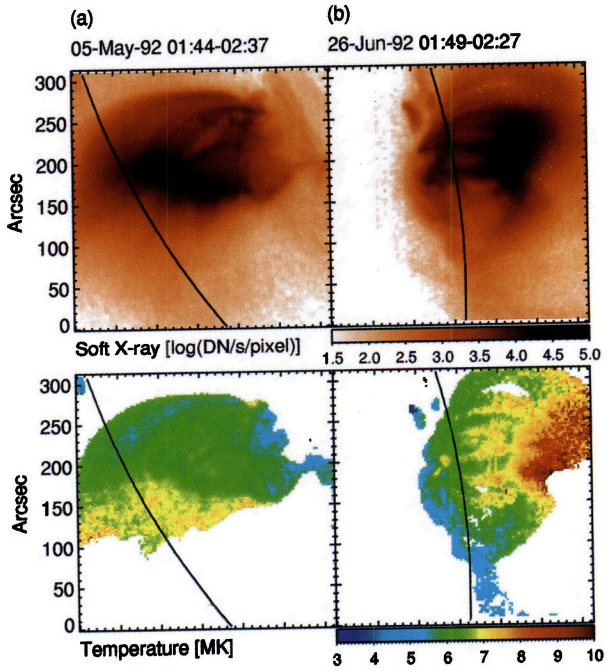

FIG. 6

FIG. 5.—Soft X-ray (thin aluminum filter) and temperature maps of the C class flare on 1992 May 5. The loop structures are heated in (*a*), followed by a clear cusp structure in (*b–e*). The solar limb position is shown by the black line.

FIG. 6.—(*a*) Soft X-ray (thin aluminum filter) and temperature maps of the M class flare on 1992 May 5. (*b*) X-class flare that occurred near the limb on 1992 June 26. In both cases, the loop-top region has the highest temperature of 7–10 MK.

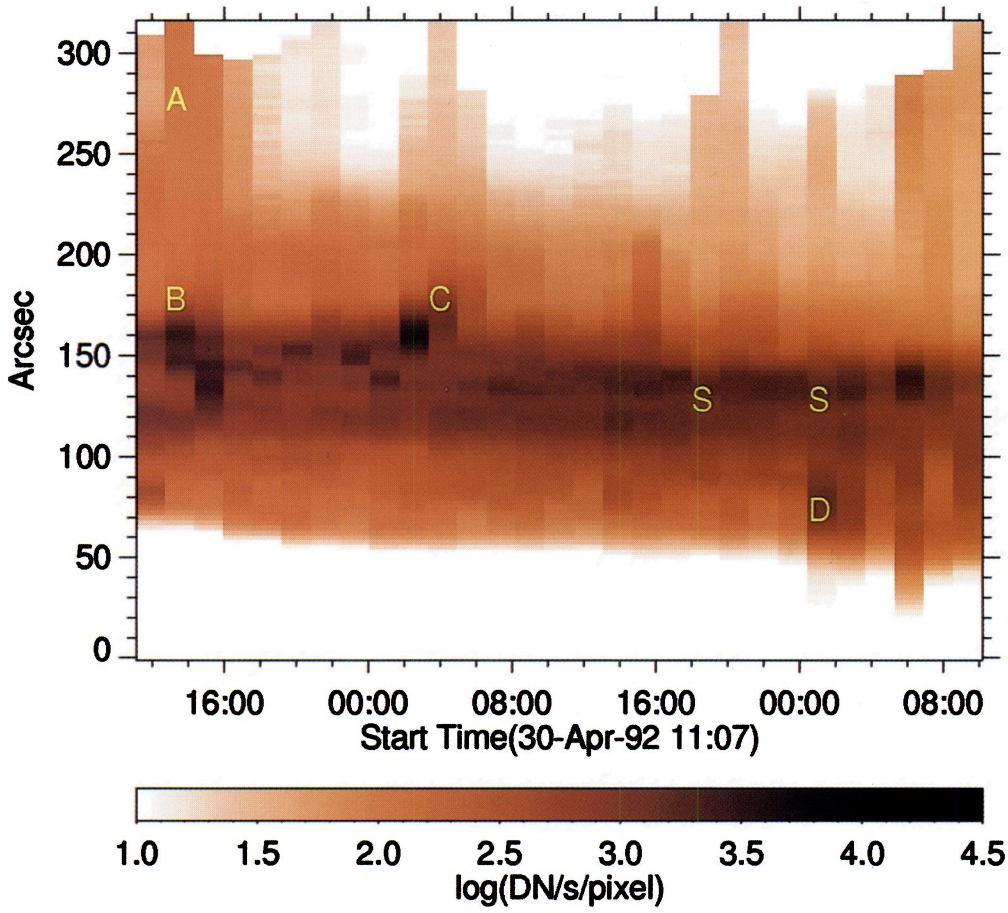

FIG. 7a

FIG. 7.—(*a*) X-ray intensity (thin aluminum filter) and (*b*) temperature along the line X shown in Fig. 2 as a function of time. The transient heatings as well as steady corona are clearly seen. The regions marked by A, B, C, and D correspond to the region with the same marks in Fig. 2.

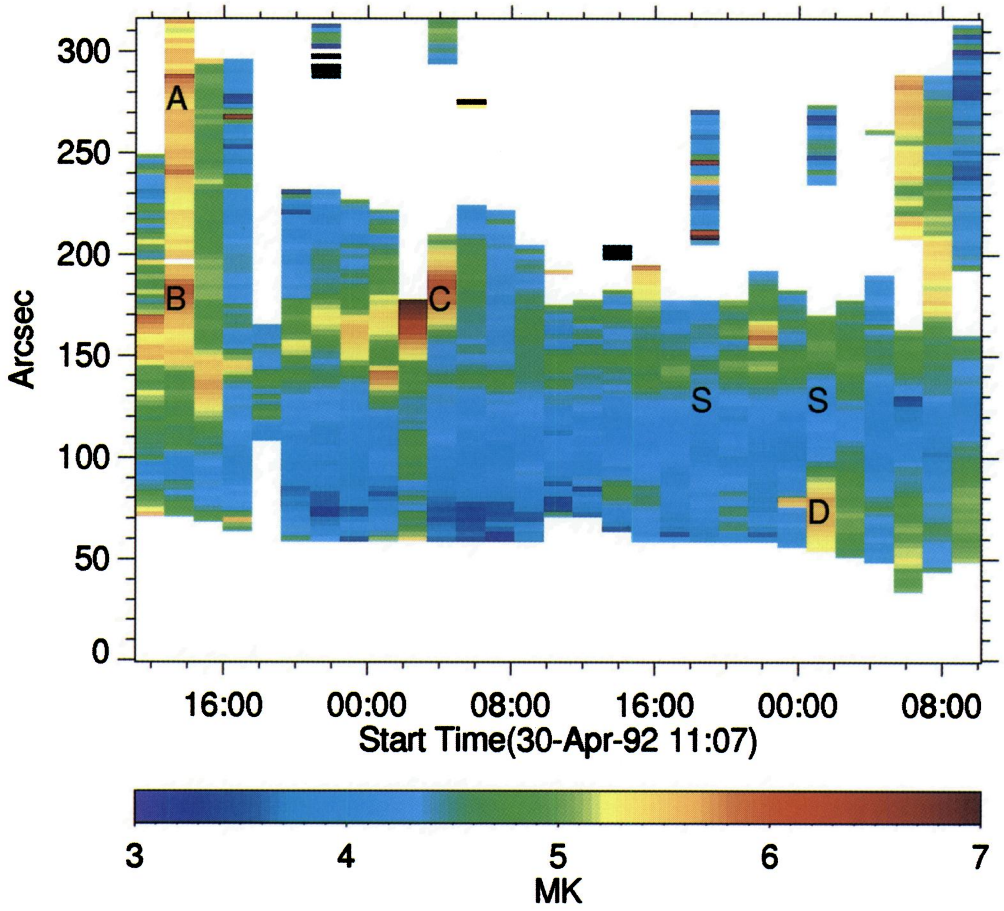

FIG. 7*b*

YOSHIDA & TSUNETA (see 459, 343)

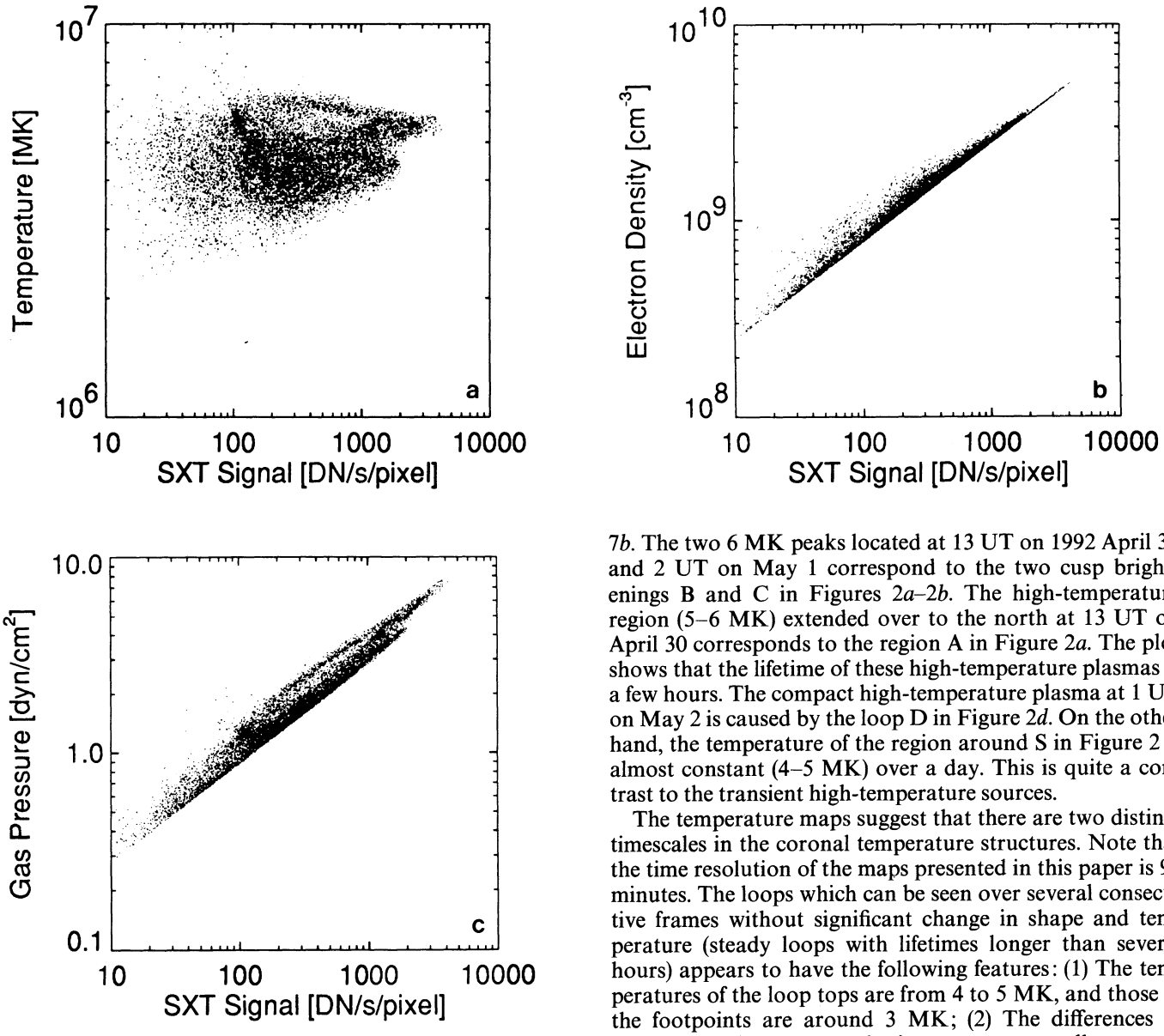

FIG. 8.—Scatter diagrams of temperature, density, and pressure with the soft X-ray intensity measured with thin aluminum filter. Each data point corresponds to each pixel of the maps in Fig. 2.

and Kano & Tsuneta (1995b). The electron density and gas pressure maps appear quite similar to the soft X-ray maps. Figure 8 shows the correlation of the temperature, density, and pressure with soft X-ray intensity (thin aluminum filter). Each data point represents a single pixel in the maps of Figure 2. These plots show that there is no correlation between the soft X-ray intensity and the temperature, whereas the density and the gas pressure are well correlated to the soft X-ray intensity: The X-ray maps can serve as density and pressure maps.

3.2. *Temperature Structure and Time Variability*

Figure 7 shows the soft X-ray intensity and the temperature along the X-axis indicated in Figure 2 as a function of time without interruption over 50 hr. Figure 7*b* clearly shows several transient heating (with time resolution of 97 minutes). The examples are A, B, C, and D in Figure 7*b*. The two 6 MK peaks located at 13 UT on 1992 April 30 and 2 UT on May 1 correspond to the two cusp brightenings B and C in Figures 2*a*–2*b*. The high-temperature region (5–6 MK) extended over to the north at 13 UT on April 30 corresponds to the region A in Figure 2*a*. The plot shows that the lifetime of these high-temperature plasmas is a few hours. The compact high-temperature plasma at 1 UT on May 2 is caused by the loop D in Figure 2*d*. On the other hand, the temperature of the region around S in Figure 2 is almost constant (4–5 MK) over a day. This is quite a contrast to the transient high-temperature sources.

The temperature maps suggest that there are two distinct timescales in the coronal temperature structures. Note that the time resolution of the maps presented in this paper is 97 minutes. The loops which can be seen over several consecutive frames without significant change in shape and temperature (steady loops with lifetimes longer than several hours) appears to have the following features: (1) The temperatures of the loop tops are from 4 to 5 MK, and those of the footpoints are around 3 MK; (2) The differences in temperature between nearby loops are too small to recognize individual loop structures in the temperature maps. The examples are the loops S in Figures 2*c*–2*d*.

On the other hand, there are loops or cusps which have time variation over adjacent images (97 minutes separation time). The properties of these transient plasmas with lifetime shorter than several hours are summarized as follows. (1) The temperatures are higher than 5 MK and do not depend on the soft X-ray intensities. For instance, the faint region A in Figure 2*a* has temperature around 6 MK. (2) The loops often have cusp structures such as loops B and C in Figure 2. Examples of the cusps are also seen in Figures 3*a*–3*b* (large cusp A in the southeast part of the active region), Figure 3*c* (small cusp B in the center), Figure 3*d* (small cusp C on the south), and Figure 3*e* (two cusps D and E on the limb). These cusp transients are not seen in the *GOES* plot and correspond to below level A–B of the *GOES* classification. The total intensity of the cusp transients is roughly similar to those of the faintest transient brightenings identified with visual inspection (Shimizu 1995). (3) The cusplike loops have higher temperatures on the outer edges than those on the inner edges. The examples are loops B and C in Figure 2.

3.3. *Transient Brightening*

Transient brightenings (Shimizu et al. 1992, 1994; Shimizu 1995) have typical lifetimes of 1–10 minutes, which is shorter than the time resolution of the temperature maps presented here. A pointlike transient brightening occurred at positon A of Figure 4 at 2255 UT on 1992 May 21. The temperature of loop B in Figure 4 increases to 7–10 MK. One of the footpoints of loop B is located just at position A. Also, we notice that faint loop C reaches a temperature of 7 MK. One of the footpoints of loop C also appears to be located at position A. Since the temperature of the faint loop C is around 5 MK in Figure 4*a*, which was taken 1.5 hr earlier than Figure 4*b*, faint loop C is also transiently heated as a result of the pointlike transient brightening. The examination of the original images shows that the X-ray intensity of loop C increases gradually over 15 minutes after the event at position A, probably owing to the evaporation of the chromospheric matter. Another example of the transient brightenings is multiple loop D in Figure 2*d*.

Transient brightenings sometimes have multiple loop structures, and Shimizu et al. (1992, 1994), Hanaoka (1994), and Arndt et al. (1994) suggested that the heating is attributable to magnetic reconnection of multiple loop structures from morphological investigation. The present observations strongly support this interpretation. The fact that two different macroscopic loop structures are significantly heated simultaneously (with time resolution of 97 minutes) can be explained by the interaction of those two separate loop structures with magnetic reconnection. It would be difficult to explain the simultaneous heating of the multiple loop without invoking magnetic reconnection of separate loop systems. The present example also shows that evidence for loop-loop interaction can be found more easily in temperature maps than in X-ray images, because those interacting high-temperature loops are more distinct with respect to the temperatures of the surrounding corona. These observations show that magnetic reconnection of different loop systems can be a strong transient heat source.

3.4. *Flare Loops and Cusp Structures*

A few flares, which have enhancements in the *GOES* X-ray monitor profile, are contained in the data set. Figure 5 shows a *GOES* C class event started at 2110 UT on 1992 May 5. The temperature of flare loop A reaches 10 MK. High-temperature cusp structure B is clearly seen in the X-ray and temperature maps through Figures 5*b*–5*e*. The top of the cusp (Fig. 5*b*) has the highest temperature (8–10 MK). Figure 6*a* shows the M class event that occurred on the east limb on 1992 May 5, and Figure 6*b* shows the X class event that occurred on the west limb on 1992 June 26. Again, the temperatures of the loop top and/or the region above the loop top are as high as 10 MK.

Similar loop-top high-temperature corona with cusp structures can be found in active regions as shown above (mini-cusp). These mini-cusps are small in energy and spatial size and are not recognized as flares in the *GOES* plot. It appears that the formation of the cusp structures contains more universal phenomena ranging from large flares to these mini-cusps. We have analyzed 400 hours of active region observations and found about 30 clear examples of cusp heating. The occurrence rate of the cusp heatings is at least two events per day for the data set.

The similarity in the morphology and the temperature structure suggests that the physical mechanism involved in the heating of the mini-cusps would be essentially the same as the large cusp-type flares (Tsuneta et al. 1992; Tsuneta 1996). The magnetic reconnection at a neutral sheet formed above the loop top would be responsible for the energy release of these mini-cusps.

4. DISCUSSION AND SUMMARY

So far, we have seen that coronal loops have a wide range of temperatures. The properties of the loops (temperatures and pressures) depend only on the present and past heating rate within the loops and do not depend on those of nearby loops. The observed wide temperature range with different timescales thus reflects a wide range of the heating profiles as a function of time.

Figure 7 shows that all the high-temperature regions (>6 MK) have lifetimes of a few hours or so. These plasmas are transiently heated. The observed decay timescale is compared with the estimated radiative and conductive timescales. (The rise time is smaller than the time resolution of the temperature maps.) The conductive timescale of these transiently heated plasmas in the corona is given by

$$t_{\rm cond} = \frac{3nk_{\rm B}Tl}{\kappa_0 T^{5/2}(T/l)}, \quad (1)$$

where $\kappa_0 T^{5/2}$ is the Spitzer thermal conductivity ($\kappa_0 = 10^{-6}$ ergs s^{-1} cm^{-1} K$^{-3.5}$; Spitzer 1962) and l is the assumed scale length of the loop. The conduction timescale $t_{\rm cond}$ is $\sim$1000–1500 s for $T = \sim$6–7 MK, $l = 10^5$ km, and $n = 10^{9.5}$ cm^{-3}. The radiative timescale is

$$t_{\rm rad} = \frac{3nk_{\rm B}T}{\Lambda(T)n^2}, \quad (2)$$

where $\Lambda(T)$ is the radiative loss function (Mewe, Gronenschild, & van den Oord 1985; Mewe, Lemen, & van den Oord 1986). Since the temperature is $T \sim$ 6–7 MK, and the radiative loss function is $\Lambda(T) = 6 \times 10^{-20}T^{-0.5} \sim 2.3$–$2.4 \times 10^{-23}$ ergs s^{-1} cm^{-3}, the radiative cooling time $t_{\rm rad}$ is 3–4×10^4 s. The observed decay timescale is close to these timescales.

The high-temperature plasma (>6 MK) are associated with the cusp structures or multiple loop structures in most cases. The transient heating is, thus, attributable to magnetic reconnection. The intensity of the cusp structures ranges from the intensity level below *GOES* B class to large X-class flare.

The loop-loop interaction is another efficient heating mechanism, as shown in Figure 4*b*. The heating of the two different magnetic loop structures strongly indicates that magnetic reconnection of multiple loops can produce heat.

The X-ray intensity has a good correlation with loop pressure and density, as shown in Figure 8. This means that we do not have good correlation between temperature and loop pressure (density). This would be the result of the time delay of the plasma filling (evaporation) for the transient heat input. If the loops or cusps are heated, the density and the pressure of the loops increase owing to the chromospheric evaporation. The evaporation proceeds essentially with dynamical timescale, the dynamical timescale (1–10 minutes) is longer than the heating timescale, and the loop filling has a time delay. If the heating is steady, the equilibrium pressure is given by the scaling law (Rosner et al. 1978; Kano & Tsuneta 1995a, b).

In addition to the transient high-temperature plasmas,

there is a definite steady plasma component. The temperature of this component is lower (3–5 MK) and has a longer lifetime ($\sim$1 day or longer). The radiative and conductive cooling timescales are 350 and 50 minutes, respectively, for $n = 10^{9.5}$ cm^{-3}, $T = 4.5$ MK, and $l = 10^{10}$ cm. The observed timescale is much longer than the conductive and radiative timescales. This indicates that the steady plasmas are continuously heated. It is sometimes hard to find the temperature structures corresponding to the steady loop structures seen in X-ray images. It appears as if individual loops lose their identity in the temperature maps. Thus, the steady coronal loops may be heated more or less in a loop-independent way. This indicates that the coronal heating consists of the basal heating and the transient heating. The basal heating mechanism maintains the plasma temperature around 3–5 MK, and the occasional transient heating owing to magnetic reconnection produces higher temperature plasma with temperatures up to 10 MK.

REFERENCES

Acton, L., et al. 1992, Science, 258, 618
Arndt, M. B., Habbal, S. R., & Karovska, M. 1994, Sol. Phys., 150, 165
Hanaoka, Y. 1994, ApJ, 420, L37
Hara, H., Tsuneta, S., Acton, L., Bruner, M., Lemen, J., & Ogawara, Y. 1994, PASJ, 46, 493
Kano, R., & Tsuneta, S. 1995a, ApJ, 454, 934
———. 1995b, PASJ, submitted
Mewe, R., Gronenschild, E. H. B. M., & van den Oord, G. H. J. 1985, A&AS, 62, 197
Mewe, R., Lemen, J., & van den Oord, G. H. J. 1986, A&AS, 63, 511
Orrall, F. Q., ed. 1981, Solar Active Regions: A Monograph from Skylab Solar Workshop III (Boulder: Colorado Associated University Press)
Rosner, R., Tucker, W., & Vaiana, G. S. 1978, ApJ, 220, 643
Shimizu, T. 1995, PASJ, 47, 251
Shimizu, T., Tsuneta, S., Acton, L., Lemen, J., Ogawara, Y., & Uchida, Y. 1994, ApJ, 422, 906
Shimizu, T., Tsuneta, S., Acton, L., Lemen, J., & Uchida, Y. 1992, PASJ, 44, L147
Spitzer, L. 1962, Physics of Fully Ionized Gases (New York: Interscience)
Tsuneta, S. 1994, in Solar Active Region Evolution, ed. K. Balasubramanian & G. Simon (San Francisco: ASP), 338
———. 1996, ApJ, in press
Tsuneta, S., Hara, H., Shimizu, T., Acton, L., Strong, K., Hudson, H., & Ogawara, Y. 1992, PASJ, 44, L63
Yoshida, T., Tsuneta, S., Golub, L., Strong, K., & Ogawara, Y. 1995, PASJ, 47, L15